Journal of Power Sources 242 (2013) 855–859

Contents lists available at SciVerse ScienceDirect

Journal of Power Sources

journal homepage: www.elsevier.com/locate/jpowsour

Short communication

Binder-free nitrogen-doped carbon nanotubes electrodes for lithium-oxygen batteries

Xiujing Lin [a], Xu Lu [a], Tao Huang [a], Zhaolin Liu [b,**], Aishui Yu [a,*]

[a] Department of Chemistry, Shanghai Key Laboratory of Molecular Catalysis and Innovative Materials, Institute of New Energy, Fudan University, 220 Handan Road, Shanghai 200438, China
[b] Institute of Materials Research and Engineering, Agency for Science, Technology and Research (A*STAR), 3 Research Link, Singapore 117602, Singapore

HIGHLIGHTS

- A simple one-step method to synthesize binder-free N-CNTs@Ni electrodes.
- The N-CNTs@Ni electrode delivers a higher capacity of 1814 mAh g^{-1} electrode.
- The unique 3-dimension network structure leads to less polarization as well as good electrochemical performance.

ARTICLE INFO

Article history:
Received 7 April 2013
Received in revised form
21 May 2013
Accepted 27 May 2013
Available online 5 June 2013

Keywords:
Lithium-oxygen batteries
Binder-free
Nitrogen-doped carbon nanotubes
Polarization

ABSTRACT

Here the binder-free nickel foam supported nitrogen-doped carbon nanotubes (N-CNTs@Ni) are synthesized by a floating catalyst chemical vapor deposition (FCCVD) method. Without any additional treatment, it could be employed as the air electrode in the lithium-oxygen batteries and delivers 1814 mAh g^{-1} (normalized to the weight of the air electrode) at the current density of 0.05 mA cm^{-2}. The loose packing 3-dimension network structure facilitates the O_2 diffusion in the inner electrode and provides enough void volume for the products deposition during discharge process. The improved contact between N-CNTs and the current collector Ni is beneficial to suppress the volume expansion and leads to less polarization as well as good cycling performance.

1. Introduction

Rechargeable lithium-oxygen batteries are considered promising for electric vehicles (EVs) and hybrid electric vehicles (HEVs) due to their extremely high energy density [1]. A prototype lithium-oxygen battery is composed of a lithium anode, organic electrolyte and a porous carbon-based electrode exposed to gaseous O_2 during cell operation. Upon discharge, Li^+ reduces O_2 to form insoluble, insulated lithium peroxide, which gradually blocks the electrolyte and oxygen pathways and eventually leads to the huge polarization and poor performance [2–4]. Therefore, the essential prerequisite for a rechargeable lithium-oxygen battery is to develop an optimum carbon electrode with appropriate morphology and structure.

To the best of our knowledge, much work has been done to explore how the morphology and structure of carbon material influence the cell performance, such as the pore diameter distribution [5,6], the thickness of the electrode [7]. In order to improve the performance of lithium-oxygen batteries, kinds of carbon have been employed in the air electrode, including high-surface area carbon material [8,9], mesocellular carbon [6], hierarchically porous honeycomb-like carbon [10], porous carbon aerogels [11] as well as graphene [2,4,12,13]. However, the porous carbon particles above are closely aggregated by a binder in the electrode and such a tight aggregation unavoidably results in the decrease in the electrode porosity [14], a low O_2-diffusion rate as well as a limited space for Li_2O_2 deposition, which consequently leads to low utilization of the carbon electrode [15]. In addition, the polyvinylidene difluoride binder (PVdF) used to fabricate the porous electrode is not stable in the presence of superoxide as well as Li_2O_2 [16–18]. Binder degradation forms a layer of LiF on the surface of the electrode, which deteriorates the clog within the electrode and reduce the space for the desired discharge product Li_2O_2. Hence, binder-free electrode design will be an effective way to avoid the formation of LiF. Intense research efforts have been focused on addressing the

* Corresponding author. Tel./fax: +86 21 51630320.
** Corresponding author.
E-mail addresses: zl-liu@imre.a-star.edu.sg (Z. Liu), asyu@fudan.edu.cn (A. Yu).

0378-7753/$ – see front matter © 2013 Elsevier B.V. All rights reserved.
http://dx.doi.org/10.1016/j.jpowsour.2013.05.100

challenges that limit the utility of lithium-oxygen batteries. Carbon nanotube/nanofiber buckpapers [7,19], all-carbon-nanofiber electrodes [20], free-standing type electrode composed of Co_3O_4 catalyst and Ni foam current collector [21], free-standing hierarchically porous carbon derived from grapheme oxide gel in nickel foam [22] have been applied in lithium-oxygen batteries, which yield high capacities and cycle performance.

Recent work has reported that nitrogen-doped carbon powder exhibits excellent electrocatalytic activity for oxygen reduction reaction and improvement to the discharge capacity [23–25]. In this work, we synthesize a new class of carbon electrodes, which are based on nitrogen-doped carbon nanotubes growing directly on Ni foam current collector (abbreviated as N-CNTs@Ni). Without the assist of binder, it could be used as the air electrode in the lithium-oxygen batteries immediately. The electrochemical examination demonstrated that the binder-free electrode delivered much higher special capacity and rate performance, comparing to the N-CNTs electrode.

2. Experimental

2.1. N-CNTs@Ni electrodes synthesis

N-CNTs@Ni electrodes were synthesized by a floating catalyst chemical vapor deposition (FCCVD) method according to the literature [25–27]. Ferrocene (99%, Aladdin) was used as the growth catalyst precursor and melamine (99%, Sinpharm Chemical Reagent Co., Ltd) was used as the nitrogen and carbon source. Typically, a mixture of 50 mg ferrocene and 1.5 g melamine in a combustion boat was placed at the upstream zone of the quartz tube (the distance from the combustion boat to a quartz-tube center: ~15 cm); a piece of Ni foam substrate was located in the center of the quartz-tube. Before the furnace was heated, Argon (99.999% in purity) was introduced into the heating system to drive the air in the tube out. Then the system was heated to 550 °C at a rate of 15 °C min^{-1} and held at the temperature for 5 min. Then the furnace was heated to 950 °C, held for 15 min and allowed to cool down to the room temperature naturally.

2.2. Physical characterization

The morphologies of binder-free N-CNT electrodes were observed by field emission scanning electron microscopy (FE-SEM, Hitachi S-4800A) and transmission electron microscopy (TEM, JEM-2100F). Structures of the as-prepared electrode were characterized by a Bruker D8 Advance X-ray diffractometer using Cu Kα radiation at a scan rate of 5° min^{-1}. A Kratos Axis Ultra X-ray photoelectron spectrometer (Al Kα source) was employed to record the XPS spectra. N_2 adsorption/desorption isotherms were obtained using a Micromeritics Tristar 3000. Fourier-transform infrared reflection (FTIR) measurements were carried out on a Shimadz IRPrestige-21 FTIR spectrometer using KBr pellet. Raman scattering spectra were constructed on a HORIBA Scientific LabRAM-1B Raman spectrometer system equipped with a 632.8 nm laser.

2.3. Electrochemical measurement

The N-CNTs@Ni electrodes were utilized in lithium-oxygen batteries without any additional binders or catalysts. For charge/discharge tests, lithium-oxygen batteries were constructed in an argon atmosphere glove box ($H_2O \leq 10$ ppm) using Swagelok batteries with an air window of 78.5 mm^2. They were assembled by stacking a Li foil, a Celgard 3500 membrane and N-CNTs@Ni electrodes. The nonaqueous electrolyte consisted of 1 M $LiPF_6$ in dimethyl sulfoxide (DMSO). Discharge/charge measurements were performed on a Land cycler (Wuhan Jinnuo Electronic Co. Ltd.) in the voltage range of 2.0–4.3 V vs. Li^+/Li at various discharge current densities.

Before each test, there was a 2 h rest to allow the batteries to reach oxygen equilibrium between the ambient environment and the electrode. All of the tests were performed at room temperature.

3. Results and discussion

3.1. Morphology and structure of the N-CNTs@Ni electrodes

As is shown in Fig. 1a, a visible black coating in the whole nickel foam was clearly observed after chemical vapor deposition. The results of XRD patterns confirmed the coating of N-CNTs. The diffraction peaks at around 26.4° correspond to (002) facet of hexagonal carbon. From the low-magnification SEM image of the N-CNTs@Ni electrode, the skeleton of Ni foam is uniformly entangled by N-CNTs. High-magnification observation showed that the diameters of the N-CNTs were on the order of 60 nm. The typical bamboo-like structure demonstrates that nitrogen was introduced into the carbon network [24]. These N-CNTs were loosely packed and formed binder-free structures, leaving large interconnected tunnels throughout the entire electrode depth. These favorable tunnels and the pores among the Ni foam facilitate oxygen diffusion during the discharge process and provide enough void volume for the discharge product deposition.

The XPS survey spectrum further confirms the successful doping of nitrogen. As is shown in Fig. 2a, three strong peaks at 286, 400, 534 eV are attributed to C 1s, N 1s and O 1s, respectively. Meanwhile, a few other peaks are observed in the survey scan, which could be assigned to Ni 3p spectrum (the small peak around 66.8 eV) and the Ni_{KLL} Auger peaks (the peaks around 481.6 eV, 460.8 eV and 409.5 eV). The high-resolution N 1s peak listed in the inset of Fig. 2b indicates that covalent C–N bonds were doped in three forms, which correspond to pyridinic N (398.6 ± 0.3 eV), pyrrolic N (400.3 ± 0.3 eV) and graphitic N (401.3 ± 0.3 eV) [28]. Primarily, nitrogen can play the role of n-type carbon dopant, which assists in the formation of disordered carbon nanostructures and therefore facilitates the ORR process [29].

Fig. 3 shows the N_2 adsorption/desorption isotherms curve of the N-CNTs@Ni electrode. Owing to the much heavier atomic weight of Ni foam, its contribution to the BET surface area could be negligible. The N_2 adsorption/desorption isotherms present type IV shape with a surface area of 42 m^2 g^{-1}. The hysteresis loop in the P/P0 range of ~0.4–1.0 is indicative of mesoporosity in addition to the presence of microporosity.

3.2. Electrochemical performance

The charge–discharge measurement was carried out in the voltage range of 2.0–4.3 V for the N-CNTs@Ni electrodes at the current densities of 0.05 mA cm^{-1}. As is shown in Fig. 4a, the N-CNTs@Ni electrodes exhibit a specific capacity of 1814 mAh g^{-1}, which are normalized to the weight of the air electrode excluding the current collector. Previous studies have been reported by fabricating the air electrode with the addition of binder and N-CNTs [24]. If all the mass of the active components (carbon + binder) in the electrode is considered, the N-CNTs electrodes deliver an initial capacity of 779 mAh g^{-1} at the current density of 75 mA g^{-1}, which is comparable to rates of 0.05 mA cm^{-2} in our work. Obviously, the N-CNTs@Ni electrodes have a much higher first specific capacity than that of N-CNTs electrode, even more than 2 times that of N-CNTs. The average discharge plateau of the N-CNT@Ni electrode is 2.68 V, higher than that of N-CNTs electrode by about 160 mV.

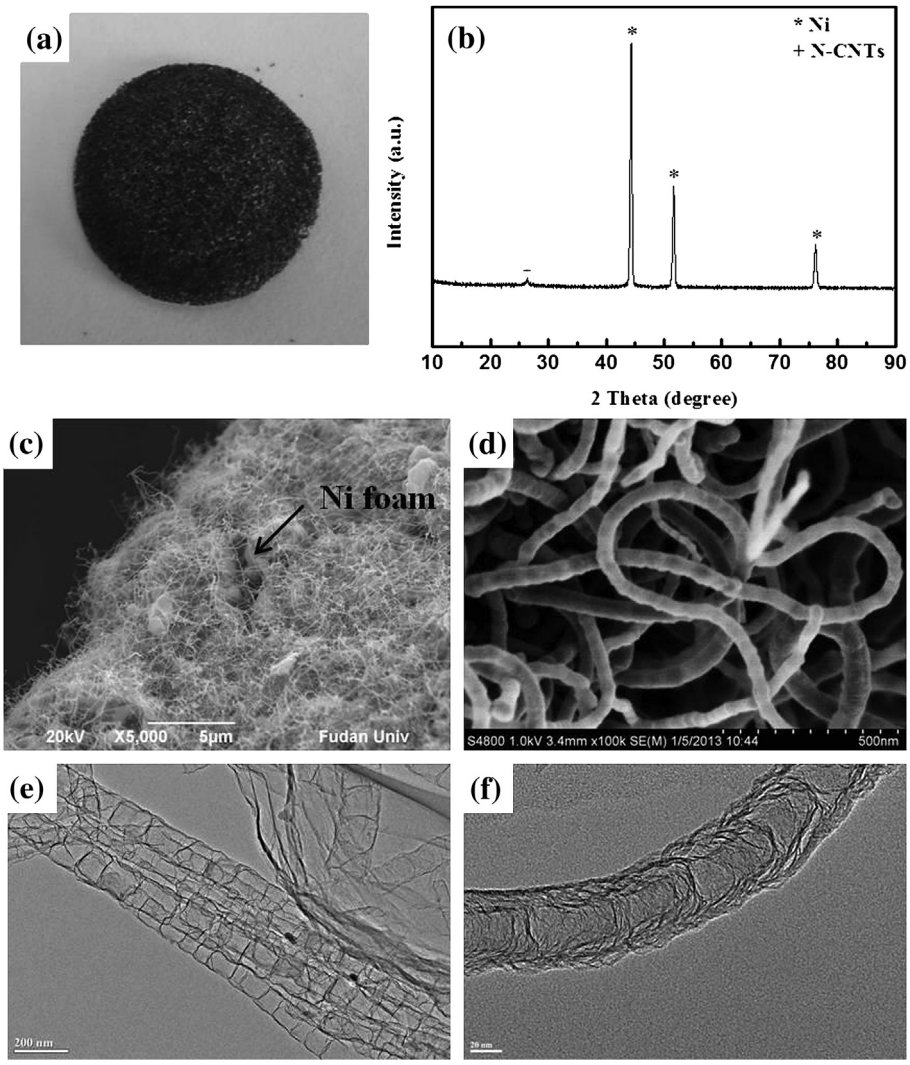

Fig. 1. (a) The photo, (b) XRD patterns, (c, d) SEM images, (e, f) TEM images of the N-CNTs@Ni electrode.

The superior performance indicates that binder-free N-CNTs@Ni substantially improved the electric contact between the carbon and the current collector Ni, which may also be beneficial to suppress the volume expansion of the electrode leading to the loss of contact between electrode particles and the current collector during constituent deposition of discharge products in conventional binder-assisted electrodes [3]. Furthermore, Fig. 4a also displays the charge behavior of the lithium-oxygen batteries with the N-CNT@Ni electrodes to the end voltage of 4.3 V. A recharge voltage plateau of 3.76 V and a recharge capacity of 922 mAh g^{-1} are obtained. However, the N-CNTs electrodes have higher average charge plateau of 4.22 V and lower capacity of 567 mAh g^{-1}. The results reflect that the N-CNTs@Ni electrode is more efficient for lessening the polarization, though it shows limited reversibility of the

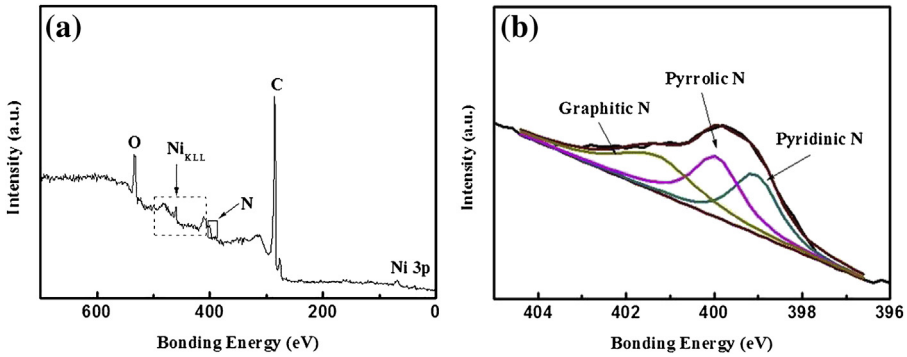

Fig. 2. (a) XPS survey spectrum, (b) N 1s spectra of the N-CNTs@Ni electrode.

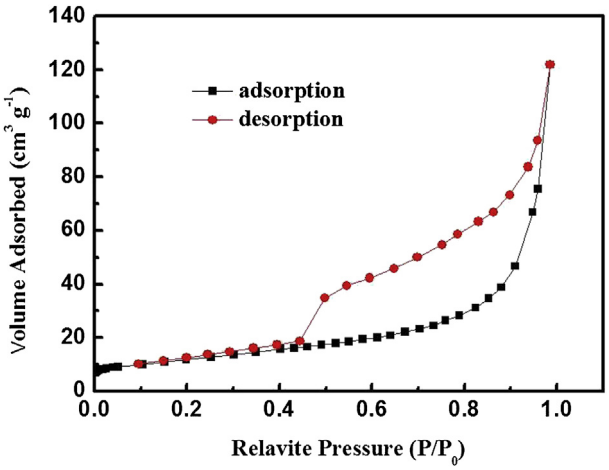

Fig. 3. N_2 adsorption–desorption isotherms of the N-CNTs@Ni electrode.

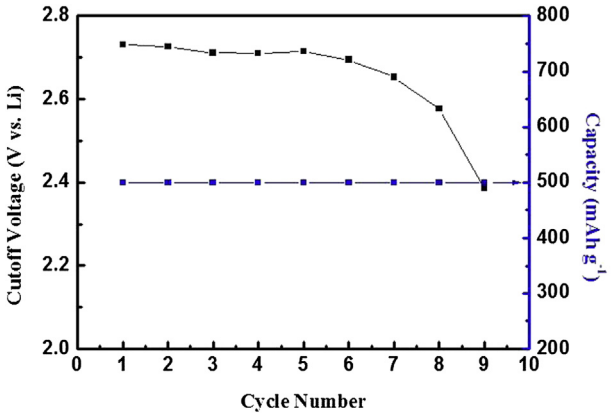

Fig. 5. Cycling performance of the N-CNTs@Ni electrode with a restriction of the capacity of 500 mAh g^{-1} at the current density of 0.05 mA cm^{-2}.

combination of the Li^+ ions from the electrolyte and e^- from the external circuit with O_2 [25,30].

The initial discharge profiles for the N-CNTs@Ni electrodes at the current densities of 0.05, 0.2, 0.5 mA cm^{-2} are shown in Fig. 4b. The initial discharge capacities initial discharge were measured to be 1814 mAh g^{-1} at 0.05 mA cm^{-1}; 798 mAh g^{-1} at 0.2 mA cm^{-1}; and 268 mAh g^{-1} at 0.5 mA cm^{-1}, respectively. While the N-CNTs electrode exhibits discharge capacities of 779 mAh g^{-1} at 0.05 mA cm^{-1}; 472 mAh g^{-1} at 0.1 mA cm^{-1}; and 337 mAh g^{-1} at 0.2 mA cm^{-1}, respectively. The discharge voltage decreases sharply with the increasing of current density, which might be due to the O_2 transport resistance in the electrolyte-filled pores of the electrode and the resistance in the solid-state diffusion of Li^+ in the ORR discharge products [31]. The electrochemical polarization becomes much more significant at high current densities and inevitably results in the rapid reduction of the discharge capacity.

The cycling performance of the N-CNTs@Ni electrodes at the current density of 0.05 mA cm^{-2} is listed in Fig. 5. By avoiding a deep discharge and restricting the capacity with a cut-off of 500 mAh g^{-1}, the N-CNTs@Ni-based battery exhibits good reversibility for 8 cycles, as the final voltage of each discharge segment stabilizes at 2.65–2.75 V. Although a decrease in the cutoff voltage is observed during cycling, the cutoff voltage of 2.44 V at the 9th cycle still remains acceptable. The cycling performance is determined by many factors, such as the Li salt, the electrolyte solvent, the catalyst the loading weight of carbon and so on. Though the cycling performance of N-CNTs@Ni electrode is not so ideal, the binder-free electrode design would be an effective method to fabrication the air cathode. Further work should be done to optimize the electrochemical performance of N-CNTs@Ni electrode in lithium-oxygen batteries.

Up to date, there are some discussions about the decomposition of the electrolyte in the lithium-oxygen batteries with carbon additive in air electrodes. The undesired reactions between the oxygen reduction intermediates and carbonate electrolyte were observed and led to quite different discharge products from Li_2O_2 [32–35]. In response to the decomposition of electrolyte, DMSO-based electrolyte was introduced [36,37]. It is established that DMSO electrolyte is not stable in contact with Li foil [38]. In order to investigate the reactivity between the two, several lithium foils were put into the DMSO electrolyte. After resting for several days, a little white precipitate was observed at the bottom of the bottle. However, according to the literature by Abraham [39], there is no such evidence of instability, which is verified by the earlier investigations of organ chemistry "Lithium wire did not react with neat DMSO at temperature up to 80 °C" [40]. It is believed that the high polarity of the DMSO solvent making it more miscible with water than many other organic solvent. In fact, it's the water mixed in the DMSO electrolyte that reacts with a lithium foil instead of DMSO itself.

FTIR measurement on the electrode before and after discharge was constructed to identify the discharge products on the N-CNTs@Ni electrode. As is shown in Fig. 6a, the formation of Li_2O_2 is observed. In addition to the peaks arising from Li_2O_2, a few small peaks are apparent in FTIR spectra, i.e., the peak at around 1420 cm^{-1} could be associated with Li_2CO_3.

Raman spectroscopy is one of the most useful techniques for identifying the discharge products in lithium-oxygen batteries. In this study *ex situ* Raman spectroscopy of the N-CNTs@Ni electrode

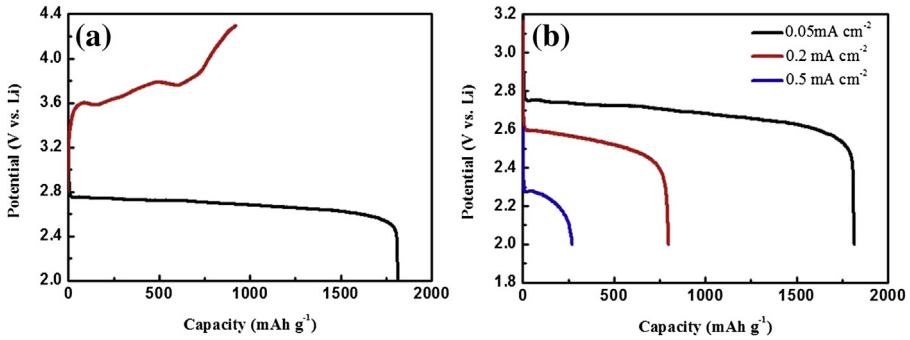

Fig. 4. (a) The charge–discharge profiles of the N-CNTs@Ni electrode at the current density of 0.05 mA cm^{-2}; (b) the discharge profiles of the N-CNTs@Ni electrode at various current densities of 0.05, 0.2, 0.5 mA cm^{-2}.

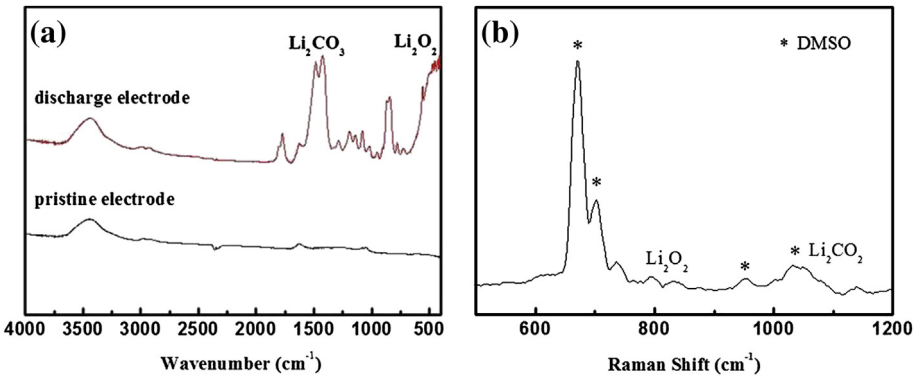

Fig. 6. (a) FTIR and (b) Raman spectra of the N-CNTs@Ni electrode at the end of discharge.

was carried out at the end of discharge. As is shown in Fig. 6b, the shoulder-like peak at around 1050 cm^{-1} corresponds to the Li_2CO_3 formation. Meanwhile, a few other peaks are observed in the Raman spectra, which could be assigned to Li_2O_2 (the peak around 790 cm^{-1}) and DMSO (the peaks around 669, 702, 952, 1035 cm^{-1}). Thereby, the *Ex situ* Raman spectroscopy measurement results suggest that both Li_2CO_3 and Li_2O_2 are generated in the case of the N-CNTs@Ni electrode. The formation of Li_2CO_3 may be due to the oxidation of the carbon material in the air electrode [38,41]. According to the literature [41], Li_2O_2 formation/decomposition is an essential prerequisite for cycling, therefore, the proportion of side-reaction products should indicate the limited reversibility of a lithium-oxygen battery.

4. Conclusions

In summary, binder-free, 3-dimensional network structure N-CNTs@Ni was synthesized successfully by a one-step method. Without any addition of binder, it could be employed as the air electrode for lithium-oxygen batteries and delivers a specific capacity of 1814 mAh g^{-1} at 0.05 mA cm^{-1}, which is more than 2 times that of N-CNTs electrode. The loose packing 3-dimension network structure facilitates the O_2 diffusion in the inner electrode and provides enough void volume for the products deposition during discharge process. The improved contact between N-CNTs and the current collector Ni is beneficial to suppress the volume expansion and leads to less polarization as well as good cycling performance.

Acknowledgments

The authors acknowledge funding supports from 973 Program (2013CB934103), the National Natural Science Foundation (No. 21173054) and Science & Technology Commission of Shanghai Municipality (No. 08DZ2270500), China.

References

[1] K. Abramham, Z. Jiang, J. Electrochem. Soc. 143 (1996) 1–5.
[2] E. Yoo, H.S. Zhou, ACS Nano 5 (2011) 3020–3026.
[3] S.S. Zhang, D. Foster, J. Read, J. Power Sources 195 (2010) 1235–1240.
[4] J. Xiao, D.H. Mei, X.L. Li, W. Xu, D.Y. Wang, G.L. Graff, W.D. Bennett, Z.M. Nie, L.V. Saraf, I.A. Aksay, J. Liu, J.G. Zhang, Nano Lett. 11 (2011) 5071–5078.
[5] C. Tran, X.Q. Yang, D.Y. Qu, J. Power Sources 195 (2010) 2057–2063.
[6] X.H. Yang, P. He, Y.Y. Xia, Electrochem. Commun. 11 (2009) 1127–1130.
[7] G.Q. Zhang, J.P. Zheng, R. Liang, C. Zhang, B. Wang, M. Hendrickson, E.J. Plichta, J. Electrochem. Soc. 157 (2010) A953–A956.
[8] J. Xiao, D.H. Wang, W. Xu, D.Y. Wang, R.E. Williford, J. Liu, J.G. Zhang, J. Electrochem. Soc. 157 (2010) A487–A492.
[9] S.D. Beattie, D.M. Manolescu, S.L. Blair, J. Electrochem. Soc. 156 (2009) A44–A47.
[10] X.J. Lin, L. Zhou, T. Huang, A.S. Yu, J. Mater. Chem. A 1 (2013) 1239–1245.
[11] M. Mirzaeian, P.J. Hall, Electrochim. Acta 54 (2009) 7444–7451.
[12] Y.L. Li, J.J. Wang, X.F. Li, D.S. Geng, R.Y. Li, X.L. Sun, Chem. Commun. 47 (2011) 9438–9440.
[13] B. Sun, B. Wang, D.W. Su, L. Xiao, H. Ahn, G.X. Wang, Carbon 50 (2012) 727–733.
[14] S.R. Younesi, S. Urbonaite, F. Björefors, K. Edström, J. Power Sources 196 (2011) 9835–9838.
[15] M. Eswaran, N. Munichandraiah, L.G. Scanlon, Electrochem. Solid-State Lett. 13 (2010) A121–A124.
[16] R. Black, S.H. Oh, J.H. Lee, T. Yim, B. Adams, L.F. Nazar, J. Am. Chem. Soc. 134 (2012) 2902–2905.
[17] R. Younesi, M. Hahlin, M. Treskow, J. Scheers, P. Johansson, K. Edström, J. Phys. Chem. C 116 (2012) 18597–18604.
[18] R. Younesi, M. Hahlin, F. Björefors, P. Johansson, K. Edström, Chem. Mater. 25 (2013) 77–84.
[19] G.Q. Zhang, J.P. Zheng, R. Liang, C. Zhang, B. Wang, M. Au, M. Hendrickson, E.J. Plichta, J. Electrochem. Soc. 158 (2011) A822–A827.
[20] R.M. Robert, M.G. Beta, V.T. Carl, S.H. Yang, Energy Environ. Sci. 4 (2011) 2952–2958.
[21] Y.M. Cui, Z.Y. Wen, Y. Liu, Energy Environ. Sci. 4 (2011) 4727–4734.
[22] Z.L. Wang, D. Xu, J.J. Xu, L.L. Zhang, X.B. Zhang, Adv. Funct. Mater. 22 (2012) 3699–3705.
[23] P. Kichambare, J. Kumar, S. Rodrigues, B. Kumar, J. Power Sources 196 (2011) 3310–3316.
[24] Y.L. Li, J.J. Wang, X.F. Li, J. Liu, D.S. Geng, J.L. Yang, R.Y. Li, X.L. Sun, Electrochem. Commun. 13 (2011) 668–672.
[25] Y.L. Li, J.J. Wang, X.F. Li, J. Liu, D.S. Geng, M.N. Banis, R.Y. Li, X.L. Sun, Electrochem. Commun. 18 (2012) 12–15.
[26] H. Liu, Y. Zhang, R. Li, X. Sun, S. Desilets, H. Abou-Rachid, M. Jaidann, L.S. Lussier, Carbon 48 (2010) 1498–1507.
[27] Z.Y. Mo, S.J. Liao, Y.Y. Zheng, Z.Y. Fu, Carbon 50 (2012) 2620–2627.
[28] G. Wu, N.H. Mack, W. Gao, S.G. Ma, R.Q. Zhong, J.T. Han, J.K. Baldwin, P. Zelenay, ACS Nano 6 (2012) 9764–9776.
[29] K. Gong, F. Du, Z. Xia, M. Durstock, L. Dai, Science 323 (2009) 760–764.
[30] Y.G. Wang, H.S. Zhou, Energy Environ. Sci. 4 (2011) 1704–1707.
[31] Y.C. Lu, G.K. David, P.C.Y. Koffi, R.H. Jonathon, J.G. Zhou, Z. Lucia, S.H. Yang, Energy Environ. Sci. 4 (2011) 2999–3007.
[32] W. Xu, V.V. Viswanathan, D.Y. Wang, S.A. Towne, J. Xiao, Z.M. Nie, D.H. Hu, J.G. Zhang, J. Power Sources 196 (2011) 3894–3899.
[33] G.M. Veith, N.J. Dudney, J. Howe, J. Nanda, J. Phys. Chem. C 115 (2011) 14325–14333.
[34] J. Xiao, J.Z. Hu, D.Y. Wang, D.H. Hu, W. Xu, G.L. Graff, Z.M. Nie, J. Liu, J.G. Zhang, 196 (2011) 5674–5678.
[35] T. Ogasawara, A. Débart, M. Holzapfel, P. Novák, P.G. Bruce, J. Am. Chem. Soc. 128 (2006) 1390–1393.
[36] Y.H. Chen, S.A. Freunberger, Z.Q. Peng, F. Bardé, P.G. Bruce, J. Am. Chem. Soc. 134 (2012) 7952–7957.
[37] D. Xu, Z.L. Wang, J.J. Xu, L.L. Zhang, X.B. Zhang, Chem. Commun. 48 (2012) 6948–6950.
[38] Z.Q. Peng, S.A. Freunberger, Y.H. Chen, P.G. Bruce, Science 337 (2012) 563–566.
[39] M.J. Trahan, S. Mukerjee, E.J. Plichta, M.A. Hendrickson, K.M. Abraham, J. Electrochem. Soc. 160 (2013) A259–A267.
[40] D.E. O'Connor, W.I. Lyness, J. Org. Chem. 30 (1965) 1620–1623.
[41] S.A. Freunberger, Y.H. Chen, Z.Q. Peng, J.M. Griffin, L.J. Hardwick, F. Bardé, P. Novák, P.G. Bruce, J. Am. Chem. Soc. 133 (2011) 8040–8047.